applied sciences

MDPI

*Article*

# Effects of Aftershocks on the Seismic Performances of Reinforced Concrete Eccentric Frame Structures

**Pengyu Sun [1,2], Weiping Wen [1,2,*] and Siwei Zhang [1,2]**

[1] Key Laboratory of Structures Dynamic Behavior and Control of the Ministry of Education, Harbin Institute of Technology, Harbin 150090, China
[2] Key Laboratory of Smart Prevention and Mitigation of Civil Engineering Disasters of the Ministry of Industry and Information Technology, Harbin Institute of Technology, Harbin 150090, China
* Correspondence: wenweiping@hit.edu.cn

**Abstract:** Strong aftershocks have the potential to cause accumulated damage in structures, a feature which has been reported in post-earthquake reconnaissance studies, particularly for eccentric or irregular structures. This study aims to investigate the seismic behaviors of eccentric RC structural models under mainshock–aftershock (MSAS) sequences. In this study, three-dimensional structural models with eccentricities of 5%, 10%, 15%, 20%, 25%, and 30%, and an eccentricity of 0 (symmetric structural model) are developed by changing the positions of the centers of the structural mass. A static pushover analysis and a nonlinear time history analysis are conducted on the structural models with different eccentricities considering unidirectional and bidirectional earthquake loading (including mainshock ground motion and MSAS sequences). The amplitude of the aftershock ground motion is scaled according to the structural damage levels calibrated with the inter-story drift ratio (IDR). Furthermore, the differences in seismic responses between the unidirectional and bidirectional eccentric structures are discussed. The results show that the peak displacements of the unidirectional eccentric structures under MSAS sequences are nearly 1.4 times higher than those under mainshock ground motions. The structural seismic responses under unidirectional earthquake loading are more sensitive to the intensity of aftershock ground motions than those under bidirectional earthquake loading. Compared with unidirectional eccentric structures, bidirectional eccentric structures are more sensitive to the intensity of aftershock ground motions and have larger torsional angles and more complex displacement trends. The maximum displacement and the maximum IDR of bidirectional eccentric structures under MSAS sequences can reach 1.5 times and 1.4 times of those under mainshock ground motions, respectively.

**Keywords:** mainshock–aftershock (MSAS) sequences; eccentricity; bidirectional earthquake loading; bidirectional eccentric structure; performance level

check for updates

**Citation:** Sun, P.; Wen, W.; Zhang, S. Effects of Aftershocks on the Seismic Performances of Reinforced Concrete Eccentric Frame Structures. *Appl. Sci.* **2023**, *13*, 10767. https://doi.org/10.3390/app131910767

Academic Editor: Jong Wan Hu

Received: 31 July 2023
Revised: 21 September 2023
Accepted: 23 September 2023
Published: 27 September 2023

**Copyright:** © 2023 by the authors. Licensee MDPI, Basel, Switzerland. This article is an open access article distributed under the terms and conditions of the Creative Commons Attribution (CC BY) license (https://creativecommons.org/licenses/by/4.0/).

## 1. Introduction

Recently, the influence of mainshock–aftershock (MSAS) sequences has gained more and more attention in earthquake engineering research. It has been observed that one principal earthquake (i.e., the mainshock) has triggered multiple aftershocks in many earthquake events, such as the Wenchuan earthquake [1] and the Tohoku earthquake [2]. The strong aftershocks have the potential to aggravate the structural damage caused by the mainshock [3,4]. It has been observed that eccentric structures are more likely to experience significant damage or collapse compared with regular structures. It has been confirmed that, in the 1972 Managua earthquake, a 15-story central bank building was severely damaged due to its stiffness asymmetry, but another 18-story Bank of America tower was only slightly damaged due to its symmetrical lateral-force-resisting system [5]. Several studies have been conducted that investigated the seismic behaviors of eccentric structures under MSAS sequences. In earlier studies, Goel and Chopra [6] and Jiang [7]

discussed the inelastic torsional response of symmetric- or asymmetric-plan systems. Reyes and Kalkan [8,9] also evaluated the significance of rotating ground motions on the behavior of multistory torsional-stiff and torsional-flexible buildings.

Structural irregularities can be divided into irregularities in plan and vertical irregularities. Some researchers have studied the seismic responses of real structures or numerical structural models with irregularities in plan. Kosmopoulos et al. [10] performed inelastic response history analyses on four real buildings with strong irregularities in plan. Buratti et al. [11] studied the seismic fragility of precast reinforced concrete buildings using observational damage data collected after the 2012 Emilia (Italy) earthquake. Ruggieri et al. [12] presented a procedure for deriving idealized 3D structures with a few degrees of freedom that matched the global response of plan-irregular, low-rise frame buildings, and then proposed some rules and equations for achieving equivalence among the linear and nonlinear properties (e.g., mass, stiffness, and strength) of the numerical models. Ruggieri et al. [13] also performed a pushover analysis on both regular and irregular RC buildings. Bhasker et al. [14] developed a seismic fragility model that was sensitive to torsional irregularity for low-rise, non-ductile RC moment frame buildings. Manie et al. [15] evaluated the damage and the collapse behavior of low-rise buildings with unidirectional mass irregularities in plan using a nonlinear static and incremental dynamic analysis (IDA), and the results showed that the adverse effects of plan irregularity on structural collapse safety were more pronounced as the number of stories increased. Some researchers have investigated the structural behavior of buildings with vertical irregularities. Michalis et al. [16] and Sayyed et al. [17] evaluated the influence of vertical irregularities on the seismic performances of steel frames and RC buildings, respectively. Han-Seon Lee [18] obtained the seismic response characteristics of three scaled 17-story RC wall building models, with different types of irregularity at the bottom two stories subjected to the same earthquake excitations. Hüseyin et al. [19] also investigated the seismic effect of structural irregularities on RC building responses by using several pushover analyses. For the earthquake excitation in the dynamic analysis of structures, more and more studies have been focused on the influence of bidirectional horizontal excitations. Pant et al. [20] investigated the effects of seismic response of a three-dimensional finite element model of a code-compliant, four-story RC building under bidirectional excitation. Kohrangi et al. [21] proposed a conditional spectrum to select bidirectional ground motions for assessing the performance of 3D structural models. Yamamoto et al. [22] conducted horizontal bidirectional loading tests for real-sized high-damping rubber bearings and compared the hysteresis loops of these bearings under bidirectional horizontal loadings with those under unidirectional loadings. Yang et al. [23] investigated the dynamic responses of two buildings connected by viscoelastic dampers under bidirectional excitations. Grant [24] also studied two horizontal ground-motion components in terms of response spectral matching. All the aforementioned studies were conducted by numerical simulation. Moreover, some researchers have investigated the torsional effect of a plan-irregular structural model through shaking table tests [25,26].

However, all the aforementioned studies have mainly focused on the seismic performance of buildings in one principal earthquake (i.e., the mainshock) and have investigated the torsional response of buildings during the mainshock. There are only a few studies that have focused on the effect of aftershocks on the structural seismic response. To the best of the authors' knowledge, the only studies aimed at MSAS sequences are summarized as follows: Hosseinpour and Abdelnaby [27] thought it was important to evaluate the effect of the direction of earthquakes' sequences, in particular, when considering the seismic behavior of irregular RC frames. Oyguc et al. [28] investigated the performance of three asymmetric-plan RC structures during the Tohoku earthquake sequences and found there was an increase in the residual drift demands for irregular RC buildings compared with regular RC structures. Nevertheless, there is still a lack of research that has systematically evaluated the seismic performance of eccentric structures or explored the influence of different eccentricities.

Based on the aforementioned discussions, this study systematically investigates the seismic behavior of typically eccentric RC structural models under MSAS sequences and discusses the influence of different eccentricities and unidirectional/bidirectional earthquake loadings on unidirectional/bidirectional eccentric structures. In this study, three-dimensional numerical models with eccentricities of 5%, 10%, 15%, 20%, 25%, and 30%, and an eccentricity of 0 (symmetric structural model) are developed by changing the positions of the structural mass centers, and they are divided into unidirectional and bidirectional structural models. For the input earthquake record, a representative mainshock–aftershock sequence is selected and scaled to different amplitudes according to the IDR, which is then applied under unidirectional and bidirectional loading. A static pushover analysis and a nonlinear time history analysis are conducted on the structural numerical models. Based on the aforementioned analysis, the seismic responses in six types of case are discussed in this study.

## 2. Numerical Modeling

### *2.1. Modeling of the Tested Structures*

In this study, according to the structural design code of China [29], a model for RC conventional frame structures with five layers, three spans, and five bays is designed. The floor height is 3.3 m. The structural model has a longitudinal span of 7.2 m and a transverse span of 6 m. Component dimensions and reinforcement information are listed in Table 1. Symmetrical three-dimensional building models are established with the OpenSEES program [30]. The Concrete02 material model is selected as the constitutive model of concrete. The model considers the tensile strength of the material and simplifies the tensioned softening branch to a linear curve, which ensures the accuracy of the calculation model and has good convergence along with high computational efficiency. The skeleton curve of the concrete in the constitutive model adopts the modified Kent–Park model [31], as shown in Figure 1. This study selected the Steel02 material model as the constitutive model of reinforcement. The Steel02 material model considers the steel tensile strength, in which the tensile softening branch is simplified as a linear processing. The model considers the effect of material strain hardening, which has been put forward by Menegotto Pinta [32] and modified by Filippou [33]. The material model also considers the Bauschinger effect. Figure 2 shows the Steel02 material monotonic envelope curves. This study used a nonlinear beam column element and fiber section in addition to the torsional section. The symmetrical building model is a three-dimensional numerical model. Each node has six degrees of freedom. The floor slab adopts a three degrees of freedom rigid diaphragm beam in OpenSEES. The floor mass is concentrated at the geometric center of the floor.

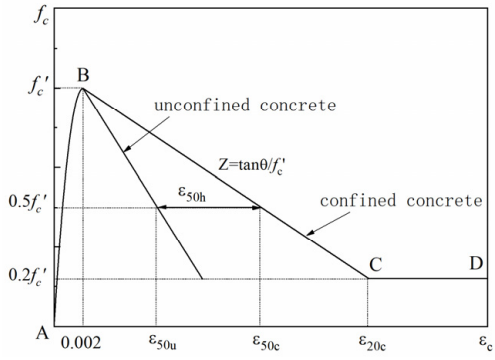



**Figure 1.** Material envelope curve models of concrete.

**Table 1.** Component dimensions and reinforcement information.

| Component | Sectional Dimension (mm × mm) | Longitudinal Bar ($mm^2$) | Hooping Bar (mm) |
|---|---|---|---|
| Beam (X direction) | 250 × 500 | Top 1140/bottom 1140 | Φ8@100 |
| Girder (Y direction) | 250 × 500 | Top 1140/bottom 1520 | Φ8@100 |
| Column | 500 × 500 | Top 942/bottom 942 | Φ10@100 |

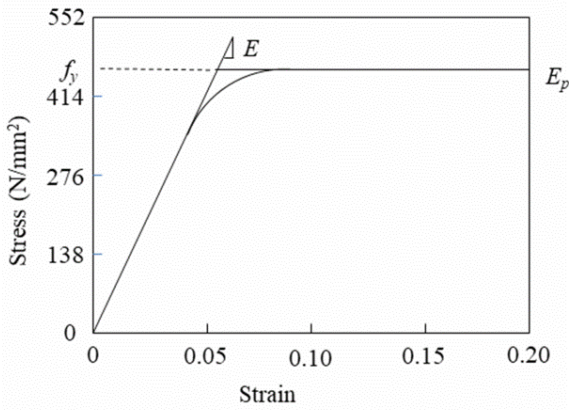



**Figure 2.** Reinforcement monotonic envelope curves.

Design load represents the combination of permanent loads and variable loads. The permanent loads include the structural self-weight, decorations, fixed equipment, and long-term storage. The variable loads include the weight of the distributed population, removable partitions, changing pipelines, and the weight of furniture placed on the floor. The combination of permanent loads and variable loads is calculated by using the following formula:

$$S_d = \mu_G S_G + \mu_{Q1} S_{Q1} + \mu_Q S_Q \quad (1)$$

where $S_d$ is the designed load value; $S_G$ and $S_Q$ are permanent loads and variable loads, respectively; $S_{Q1}$ is the main controlled variable load; $\mu_G$ and $\mu_Q$ are combined factors for permanent loads and variable loads, which are 1.2 and 0.7, respectively; $\mu_{Q1}$ is the combined factor for main controlled variable load, which is 0.98.

On the basis of the symmetric structural model, mass eccentric structural models are developed. Generally, the eccentric structural models are divided into "mass eccentricity models" and "rigidity eccentricity models". In this study, the mass eccentricity model is chosen to characterize structural eccentricity, which is used to represent a wide range of situations including probable distribution of furniture load, personnel distribution, equipment installation, construction error, and so on. To achieve different eccentricities in the structural models, the mass concentration point (i.e., floor mass center) of each floor is continuously shifted along the horizontal direction. The floor rigidity center remains unchanged. Then, the models will have different eccentricities with the movement of the mass concentration point. Moreover, with the eccentricity adjustments, there are no changes in other building parameters, including floor mass and floor stiffness distribution. Thus, the only variable that affects the torsional response is eccentricity.

The material parameters of the concrete and steel reinforcement in the structural models are listed in Table 2. These parameters are requested in Concrete02 and Steel02 material models in the OpenSees.

In this research, there are uniaxial eccentric structural models and bidirectional eccentric structural models in the dynamic time history analyses. The eccentricities of both types of models are set as 0%, 5%, 10%, 15%, 20%, 25%, and 30% (0% eccentricity corresponds to the symmetric structural model). In the bidirectional eccentric structural models, the eccentricities in the X and Y directions are the same. Figures 3 and 4 show the layouts of the uniaxial eccentric structure and the biaxial eccentric structure.

**Table 2.** Material parameters of the concrete and steel reinforcement in the structural models.

| Material | Maximum Stress $f_c$ (MPa) | Strain at Maximum Stress $\varepsilon_0$ | Ultimate Stress $f_u$ (MPa) | Strain at Ultimate Stress $\varepsilon_u$ | Ratio between Unloading Slope and Initial Slope $\lambda$ | Tensile Strength $f_t$ (MPa) | Tension Softening Stiffness $E_t$ (MPa) |
|---|---|---|---|---|---|---|---|
| Unconfined concrete | −27.4 | −0.003 | −5.5 | −0.01 | 0.1 | 2.7 | $1.4 \times 10^3$ |
| Confined concrete | −35.6 | −0.006 | −7.1 | −0.012 | 0.1 | 3.6 | $1.8 \times 10^3$ |
| | **Yield stress *Fy* (MPa)** | **Modulus of steel $E_s$ (MPa)** | **Strain-hardening ratio $b_s$** | **Parameter R0** | **Parameter cR1** | **Parameter cR2** | |
| Steel | 457 | $2 \times 10^5$ | 0.01 | 18 | 0.925 | 0.15 | |

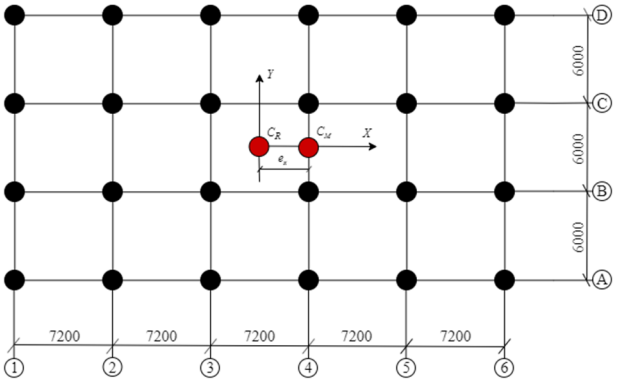



**Figure 3.** Plan and layout of the uniaxial eccentric structure.

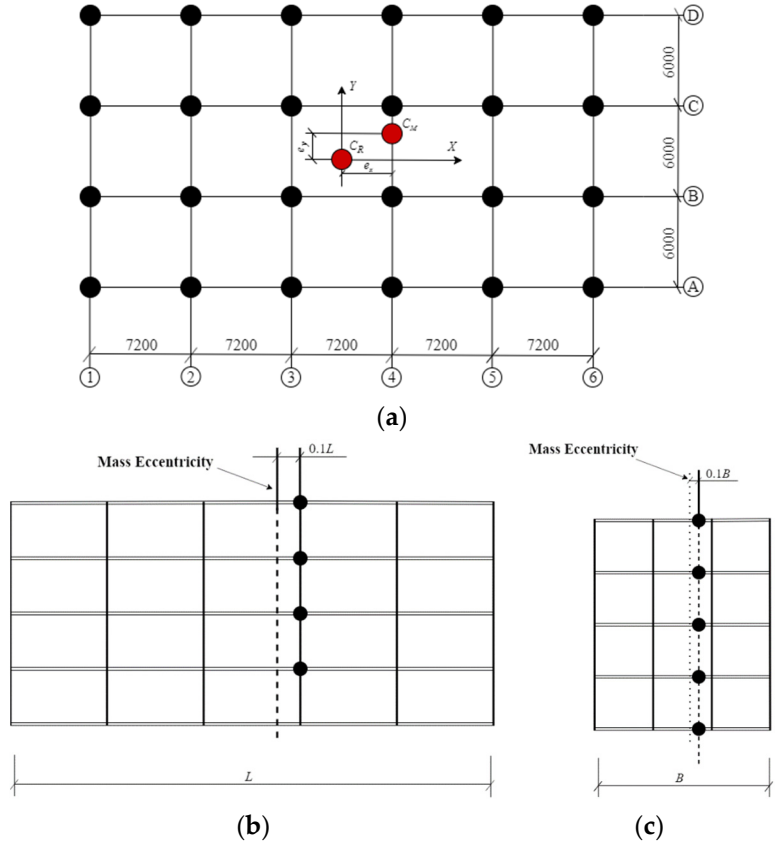



**Figure 4.** Plan and vertical layout of the biaxial eccentric structure: (**a**) Plan layout; (**b**) vertical layout of the biaxial eccentric structure in the X direction; (**c**) vertical layout of the biaxial eccentric structure in the Y direction. Note: CM is the center of mass and CR is the rigidity center.

The eccentricity is obtained by using Equation (2):

$$\omega_i = e_i / L_i \quad (2)$$

where $\omega_i$ denotes the eccentricity of the structural model and $e_i$ denotes the eccentric distance, which is the distance between the mass center and rigidity center. $L_i$ denotes the building outline length in eccentric direction.

For mass eccentric structural models, the basic assumptions are as follows:

(a) Each floor is a rigid floor.
(b) The total mass and moment of inertia of each floor are appointed at the geometric center of the floor.
(c) Each floor has three degrees of freedom (two translational degrees of freedom and one rotational degree of freedom).
(d) The torsional stiffness of the structure is elastic.
(e) The centers of stiffness are basically located at the geometric center of each story, present on the same vertical axis. The floor stiffness distribution could be regarded as uniform and symmetric.
(f) The influence of the non-synchronous nonlinear behavior of different columns on the change in eccentricities is not considered in this study.

### 2.2. Vibrational Characteristic Analysis

To calculate the natural frequencies and modes of the structures, eigenvalue analyses are performed for all the structural models in OpenSEES. The first five vibration periods of both the uniaxial eccentric structural models and the bidirectional eccentric structural models are listed in Tables 3 and 4, respectively. The first two modes of the structures are translational modes, and the third mode is the torsional mode. The translational–torsional period ratio is the ratio of the translational mode period to the torsional mode period, which is also the ratio of the first period to the third period. With an increase in eccentricity, the fundamental periods of the structures gradually rise, and the translational–torsional period ratios also become higher. Moreover, the second mode period remains stable no matter what the eccentricity is. It can also be observed from Tables 3 and 4 that the first mode periods of the bidirectional eccentric structural models exceed those of the corresponding uniaxial eccentric structural models. Consequently, translational–torsional period ratios of bidirectional models are greater than those of uniaxial models.

**Table 3.** The first five vibration periods of the uniaxial eccentric structural models.

| Mode | Eccentricity (%) | | | | | | |
|---|---|---|---|---|---|---|---|
| | 0 | 5 | 10 | 15 | 20 | 25 | 30 |
| 1 | 1.169 | 1.169 | 1.195 | 1.244 | 1.306 | 1.380 | 1.462 |
| 2 | 1.152 | 1.163 | 1.170 | 1.169 | 1.169 | 1.169 | 1.169 |
| 3 | 0.770 | 0.766 | 0.756 | 0.742 | 0.726 | 0.712 | 0.698 |
| 4 | 0.328 | 0.328 | 0.338 | 0.354 | 0.374 | 0.397 | 0.423 |
| 5 | 0.323 | 0.327 | 0.328 | 0.328 | 0.328 | 0.328 | 0.328 |
| Translational–torsional period ratio | 1.518 | 1.526 | 1.581 | 1.677 | 1.791 | 1.938 | 2.094 |

Since there are no differences in the total mass and stiffness distribution among different eccentricity models, there is only one parameter to change, which is eccentricity. Therefore, the period is considered to be a function of eccentricity. Since the vibration of the structure is controlled by the translational mode and the torsional mode, in this study, the formulas for the first and third periods and eccentricity, respectively, are shown in Equations (3)–(6). Equations (3) and (4) are subjected to the first mode and third mode in Table 3, and Equations (5) and (6) are subjected to the first mode and third mode in Table 4.

$$T = 3 \times 10^{-4}\omega^2 + 4 \times 10^{-4}\omega + 1.164 \; R^2 = 0.9981 \quad (3)$$

$$T = 3 \times 10^{-6}\omega^3 - 2 \times 10^{-4}\omega^2 - 1 \times 10^{-4}\omega + 0.7701 \; R^2 = 0.999 \quad (4)$$

$$T = 4 \times 10^{-4}\omega^2 + 1.4 \times 10^{-3}\omega + 1.164 \; R^2 = 0.998 \quad (5)$$

$$T = 3 \times 10^{-6}\omega^3 - 2 \times 10^{-4}\omega^2 - 2 \times 10^{-4}\omega + 0.7701 \; R^2 = 1 \quad (6)$$

**Table 4.** The first five vibration periods of the bidirectional eccentric structural models.

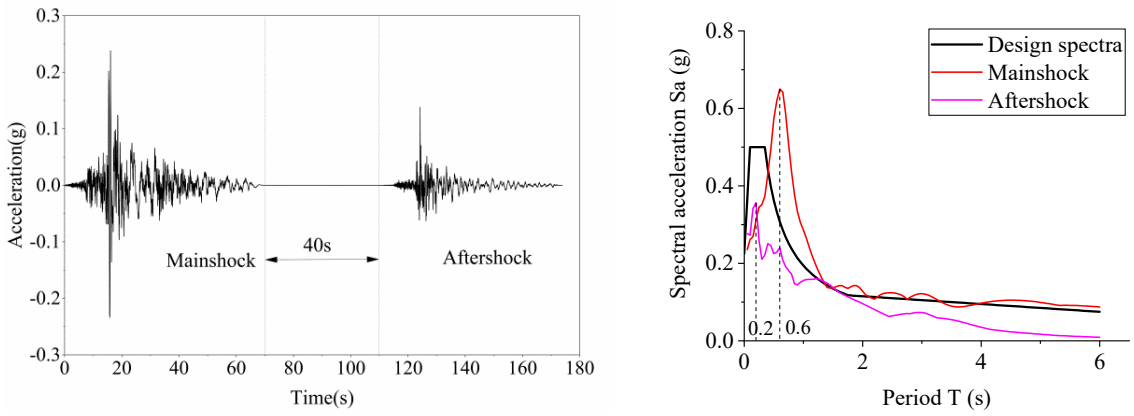
| Mode | Eccentricity (%) | | | | | | |
|---|---|---|---|---|---|---|---|
| | 0 | 5 | 10 | 15 | 20 | 25 | 30 |
| 1 | 1.169 | 1.175 | 1.209 | 1.268 | 1.342 | 1.430 | 1.528 |
| 2 | 1.152 | 1.161 | 1.165 | 1.166 | 1.166 | 1.166 | 1.166 |
| 3 | 0.770 | 0.765 | 0.753 | 0.737 | 0.720 | 0.704 | 0.691 |
| 4 | 0.328 | 0.330 | 0.342 | 0.362 | 0.386 | 0.413 | 0.443 |
| 5 | 0.323 | 0.326 | 0.327 | 0.327 | 0.327 | 0.327 | 0.327 |
| Translational–torsional period ratio | 1.518 | 1.536 | 1.606 | 1.720 | 1.864 | 2.031 | 2.211 |

### *2.3. Ground Motion Selection and Scaling*

In this research, a recorded MSAS ground motion from the 1999 CHICHI earthquake, whose information is summarized in Table 5, was selected as the representative earthquake input for the dynamic analysis. The CHICHI earthquake was a very famous earthquake that occurred in Taiwan. Rich ground motion records were obtained, and, after the mainshock, there were many recorded aftershocks. Many mainshock–aftershock sequences were recorded at the same station in orthogonal directions. Therefore, a representative mainshock–aftershock sequence recorded at the CHY029 station in direction N was selected. The acceleration time history is shown in Figure 5a. In this manuscript, for simplicity and consistency, "CHICHI-CHY029-N" is used to designate this earthquake.

**Table 5.** Information of the selected mainshock and aftershock earthquake records.

| Earthquake Name | Type | Station | Direction | Time | $M_w$ | PGA |
|---|---|---|---|---|---|---|
| CHICHI | Mainshock | CHY029 | N | 20 September 1999 | 7.62 | 0.238 g |
| | Aftershock | CHY029 | N | 25 September 1999 | 6.30 | 0.158 g |




(**a**) (**b**)

**Figure 5.** The records of CHICHI-CHY029-N mainshock and aftershock: (**a**) The acceleration time history; (**b**) spectral acceleration.

Figure 5b shows the design spectra and acceleration response spectra of the mainshock and aftershock. The design spectra are based on the Chinese seismic design code [29], where the maximum acceleration coefficient is 0.5. The mainshock and aftershock records are scaled to rare earthquake level in degree 7. As shown in Figure 5b, the periods corresponding to maximum spectral acceleration of mainshock and aftershock records are 0.2 s and 0.6 s, respectively.

The amplitudes of the mainshock and aftershock are scaled according to the following method. The peak acceleration (PGA) of the recorded mainshock earthquake is 0.238 g, and that of the aftershock is 0.158 g. The maximum IDR is more sensitive to the intensity of the aftershock ground motion as compared with other structural response indicators, which is due to the dynamic analysis results that the structural IDR most obviously changes with the structural eccentricity. Therefore, the IDR was selected as an amplification factor for earthquakes. The performance level and the corresponding IDR are listed in Table 6, as recommended in FEMA 2000. When the structural IDR reaches 1%, 2%, and 4%, the mainshock PGA is calculated to be 0.15 g, 0.25 g, and 0.32 g, respectively. For each mainshock PGA, the amplitude of the aftershock is scaled by 0.6, 0.8, 0.9, and 1 times the amplitude of the mainshock. Table 6 shows the proportional PGA values of the mainshock and aftershock at different damage levels. It is worth mentioning that for consistency, all the cases of mainshock amplitudes are calculated and determined based on symmetric structural models. A time interval of 40 s between the mainshock and aftershock is added into the program to calm the model vibration after the mainshock loading.

**Table 6.** Scaled PGAs of the mainshock and aftershock for different damage levels of the CHI-CHI-CHY029-N earthquake record.

| Performance Level | Damage Description | $PGA_{ms}$ | $PGA_{as}/PGA_{ms}$ | $PGA_{as}$ |
|---|---|---|---|---|
| Immediate occupancy | Maximum IDR is 1% | 0.15 g | 0.6 | 0.09 g |
| | | | 0.8 | 0.12 g |
| | | | 0.9 | 0.135 g |
| | | | 1 | 0.15 g |
| Life safety | Maximum IDR is 2% | 0.25 g | 0.6 | 0.15 g |
| | | | 0.8 | 0.2 g |
| | | | 0.9 | 0.225 g |
| | | | 1 | 0.25 g |
| Collapse prevention | Maximum IDR is 4% | 0.32 g | 0.6 | 0.192 g |
| | | | 0.8 | 0.256 g |
| | | | 0.9 | 0.288 g |
| | | | 1 | 0.32 g |

## 3. Results and Discussion

### 3.1. Spatial Pushover Analysis (SPA)

A pushover analysis is applied to the tested eccentric structures in this section. The lateral loads are assigned to the mass center of each floor. The roof displacements and first floor displacements of the eccentric structures of different eccentricities under lateral load are shown in Figure 6a,b, respectively. The resistance force decreases as the eccentricity increases, which means the seismic capacity of the structure is weaker. The structure with 5% eccentricity is an exception. The structure with 0% eccentricity (i.e., a symmetrical structure) has the best seismic capacity, and the structure with 30% eccentricities has the worst seismic capacity.

### 3.2. Seismic Dynamic Analyses of Unidirectional Eccentric Structures

In this section, the nonlinear time history analyses of the unidirectional eccentric structural and bidirectional eccentric structural models are presented. The details of all models used in the research are described in Section 2. A total of six cases are explored, as shown in Table 7. Firstly, the dynamic analysis of the unidirectional eccentric structure under unidirectional seismic load is carried out, i.e., the UUM situation shown in Table 7. In

this study, several structural response parameters in the UUM analysis are compared, and the most sensitive response parameters to eccentricity are selected as the criteria indicators in earthquake amplitude modulation. These are used in the dynamic analysis subjected to MSAS sequences.

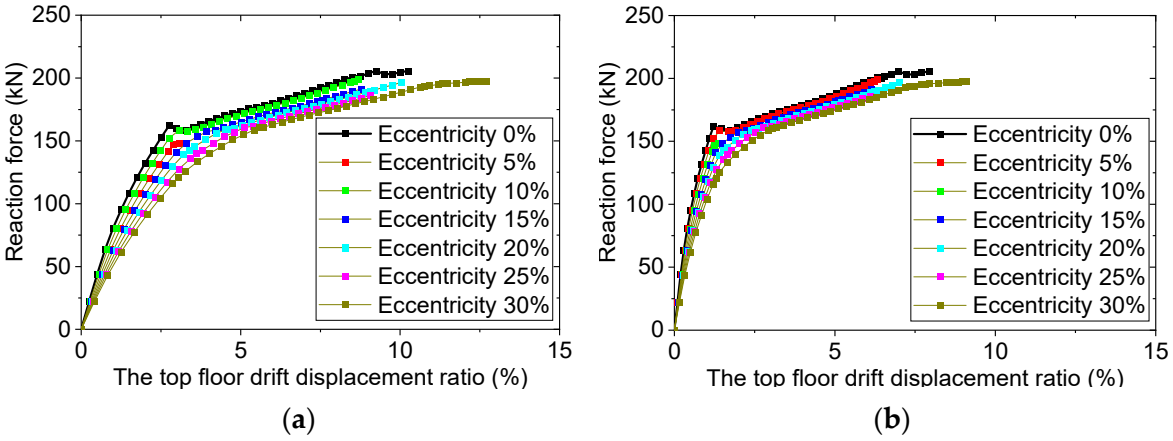



**Figure 6.** The results of the pushover analysis: (**a**) Top floor drift displacement ratio; (**b**) first floor drift displacement ratio.

**Table 7.** Seismic dynamic analyses of eccentric structures.

| No | Structure | Load | Abbr. |
|---|---|---|---|
| 1 | Unidirectional eccentric structure | Unidirectional mainshock ground motion | UUM |
| 2 | Unidirectional eccentric structure | Unidirectional mainshock–aftershock sequences | UUS |
| 3 | Unidirectional eccentric structure | Bidirectional mainshock ground motion | UBM |
| 4 | Unidirectional eccentric structure | Bidirectional mainshock–aftershock sequences | UBS |
| 5 | Bidirectional eccentric structure | Bidirectional mainshock ground motion | BBM |
| 6 | Bidirectional eccentric structure | Bidirectional mainshock–aftershock sequences | BBS |

3.2.1. Response of the Unidirectional Eccentric Structure under Unidirectional Mainshock

In order to find the structural seismic response parameters that are most sensitive to structure eccentricity, a dynamic time history analysis of unidirectional eccentricity under the ground motion records of the mainshock (Case UUM) was carried out. Taking the ChiChi-CHY029-N earthquake record as an example, the acceleration time history of the mainshock record is shown in Figure 7. The amplitude of the mainshock adopts the actual recorded PGA, i.e., 0.238 g. The unidirectional eccentric structural model is symmetric in the X direction and eccentric in the Y direction, with eccentricities of 0%, 5%, 10%, 15%, 20%, 25%, and 30%. Only the Y direction is utilized to input ground motion. The running time of the program (110 s) is 40 s longer than the ground motion time, which is used to calm the structural vibration after the mainshock.

The response results, including maximum displacements in the X and Y directions, the maximum residual displacement, the torsional angle, the relative torsional effect, and the maximum IDR, are extracted and compared. The maximum displacements of structural models in the Y direction under all eccentricities are shown in Figure 8a. It is evident that as eccentricity increases, the structural displacement also increases, and the increasing speed exhibits a pattern of at first rapid and then slow growth. This indicates that the influence of eccentricity on displacement will gradually weaken with an increase in eccentricity. The maximum increase was more than 2.5 times, at 30% eccentricity.

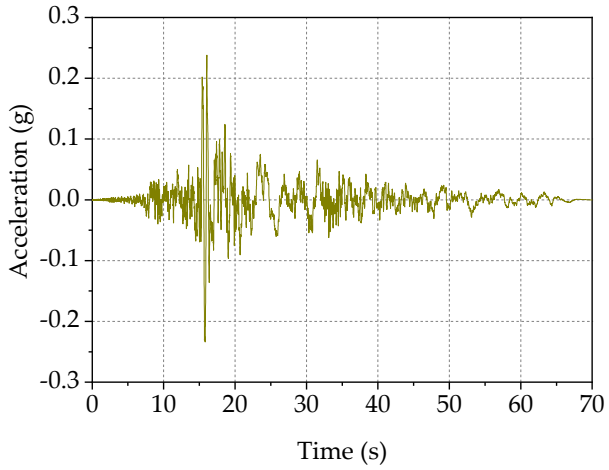



**Figure 7.** Acceleration time history of the CHICHI-CHY029-N mainshock record.

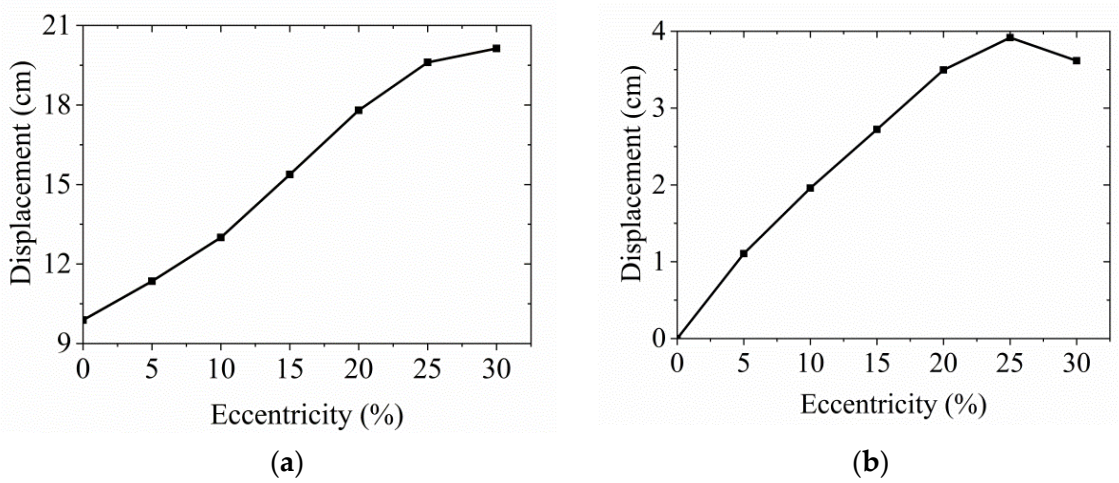



**Figure 8.** Maximum displacements of structural models in: (**a**) the Y direction; (**b**) the X direction.

In the X direction, another horizontal direction perpendicular to the Y direction of earthquake loading, the effect of ground motion is very small and almost negligible for the symmetrical structure, as shown in Figure 8b. When the structure produces eccentricity, even if the eccentricity is 5%, a displacement of more than 10 mm can be generated, which is about 1/10 of the Y direction displacement. With an increase in eccentricity, the X direction displacement of the structure becomes larger and larger, showing linear growth until the eccentricity reaches 25%. When the eccentricity continues to increase to 30%, the displacement growth trend slows down in the Y direction. It is anticipated that the displacement decreases in the X direction, possibly as a result of the structure's plane–torsion coupling reaction, which also reflects the complexity of the eccentric structure's torsional response as compared to the symmetric structure's response.

In Figure 9, the residual displacements of the structural models show a small fluctuation in certainty scope before the eccentricity rate of 15%. When the eccentricity is in the range of 15–30%, the residual displacement of the structure ascends rapidly, which reflects the structure going into plastic status. Figure 10 shows the trend of the torsional angles for all of the structural models. The torsional angle is one of the important indicators to evaluate the torsional effect of the structure. The torsional angle steadily increases with increasing eccentricity and increases approximately linearly when the eccentricity is between 0% and 15%. The growth rate decreases when the eccentricity is in the range of 15–25%, but the slope is negative after surpassing an eccentricity of 25%. It clearly presents

the process that the structure follows from the elastic stage to the plastic stage and its finally destruction with the rise in eccentricity.

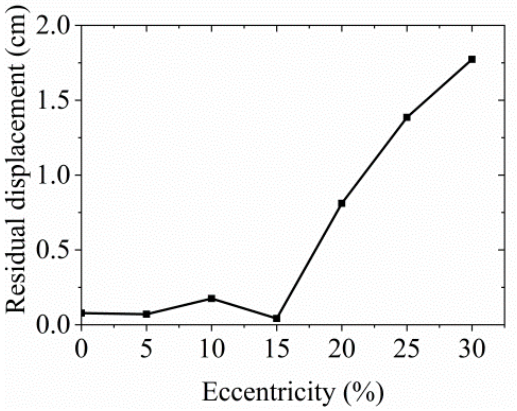



**Figure 9.** Residual displacements of the top floor of the structural models in the Y direction.

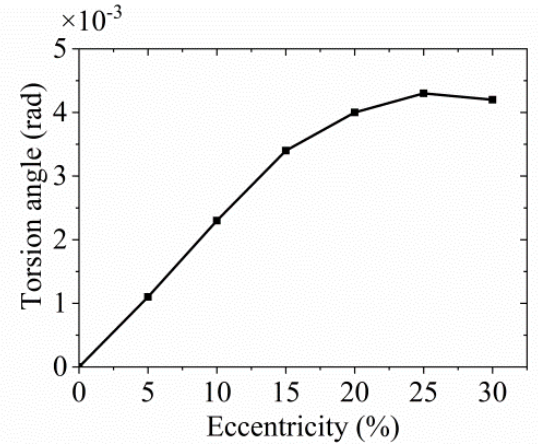



**Figure 10.** Torsional angles of the structural models.

Figure 11 shows the moving trend of relative torsional effect with a change in eccentricity. The relative torsional effect $\gamma$ is defined as the ratio of the displacement at the radius of rotation from the rigid center to the translational displacement of the floor. It reflects the ratio of the torsional displacement to the translation displacement of the structure due to torsion and is one of the important indexes to measure the torsional effect for eccentric structures. It is calculated by Equation (7):

$$\gamma = \theta r / u \tag{7}$$

where $\theta$ refers to the torsional angle of the characteristic point which is located at the radius of rotation from the rigid center. Herein, since a rigid floor is adopted in these models, $\theta$ is the torsional angle of the whole floor. The parameter $r$ is the radius of rotation, i.e., the distance between the center of mass and the rigid center in these models. The parameter $u$ is the horizontally lateral displacement of the floor in the direction of seismic loading.

At low eccentricities (eccentricity 0–10%), the relative torsional effect rises gradually; however, from 10% eccentricity, it rises quickly, with an almost linear trend. Then, the relative torsional effect appears to slow the growth rate as it approaches the high eccentricity region (eccentricity 25–30%). In contrast to the maximum IDR, the relative torsional effect exhibits a similarly linear upward trend with increasing eccentricity, but it is unable to accurately and broadly characterize the extent of damage in all structures. The relative torsional effect is zero in the symmetric structural model; however, it does not depict that

there is absolutely no damage at that time. Moreover, it needs to be calculated extensively rather than obtained directly by measuring or by a simple calculation such as an inter-story drifts ratio. Therefore, in this study, the maximum IDR is selected as the criteria indicator in earthquake scaling, as shown in Table 7, and it is used as the response indicator in the later seismic analysis work subjected to mainshock–aftershock sequences.

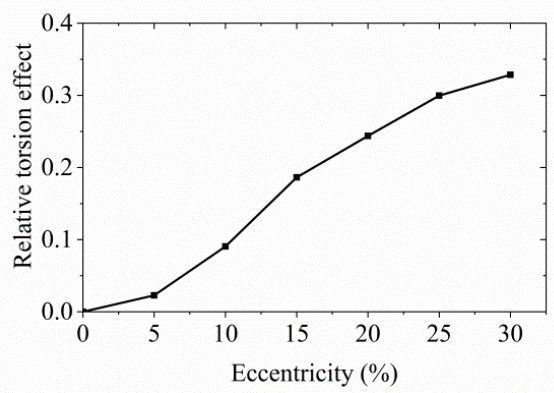



**Figure 11.** Relative torsional effects of the structural models.

Moreover, the maximum IDRs in the Y direction for symmetrical and eccentric structural models is obtained in the study, as shown in Figure 12. For each model, the largest IDR appears at the bottom layer. With the improvement in eccentricity, the IDR becomes larger and larger for the first floor. This illustrates that the bottom of structures is most influenced by eccentricity, and the maximum IDR is the most sensitive indicator for the increase in eccentricity. Moreover, the maximum IDR is considered to be an intuitive observation indicator of structural deformation in many national codes. It can directly present the structural damage phenomenon in the failure process. This is another justification for choosing the maximum IDR as the scaled criterion indicator in this study, as shown in Table 7.

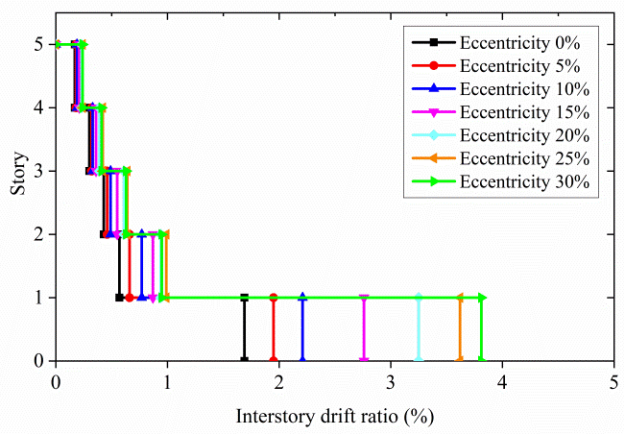



**Figure 12.** Maximum IDR of structural models in the Y direction.

### 3.2.2. Responses of the Unidirectional Eccentric Structure under Unidirectional Mainshock–Aftershock Sequences

In this section, the seismic responses of the unidirectional eccentric structure under unidirectional mainshock–aftershock sequences (Case UUS) are investigated. The influences of aftershock and the eccentricity of structures on the seismic responses are discussed.

Figure 13 shows the seismic responses of structures under mainshock–aftershock sequences with different mainshock PGAs, including maximum displacement (as shown in Figure 13a,c,e) and IDR (as shown in Figure 13b,d,f). For each mainshock PGA, the PGA of the aftershock is scaled to 0.6, 0.8, 0.9 and 1.0 times that of the mainshock.

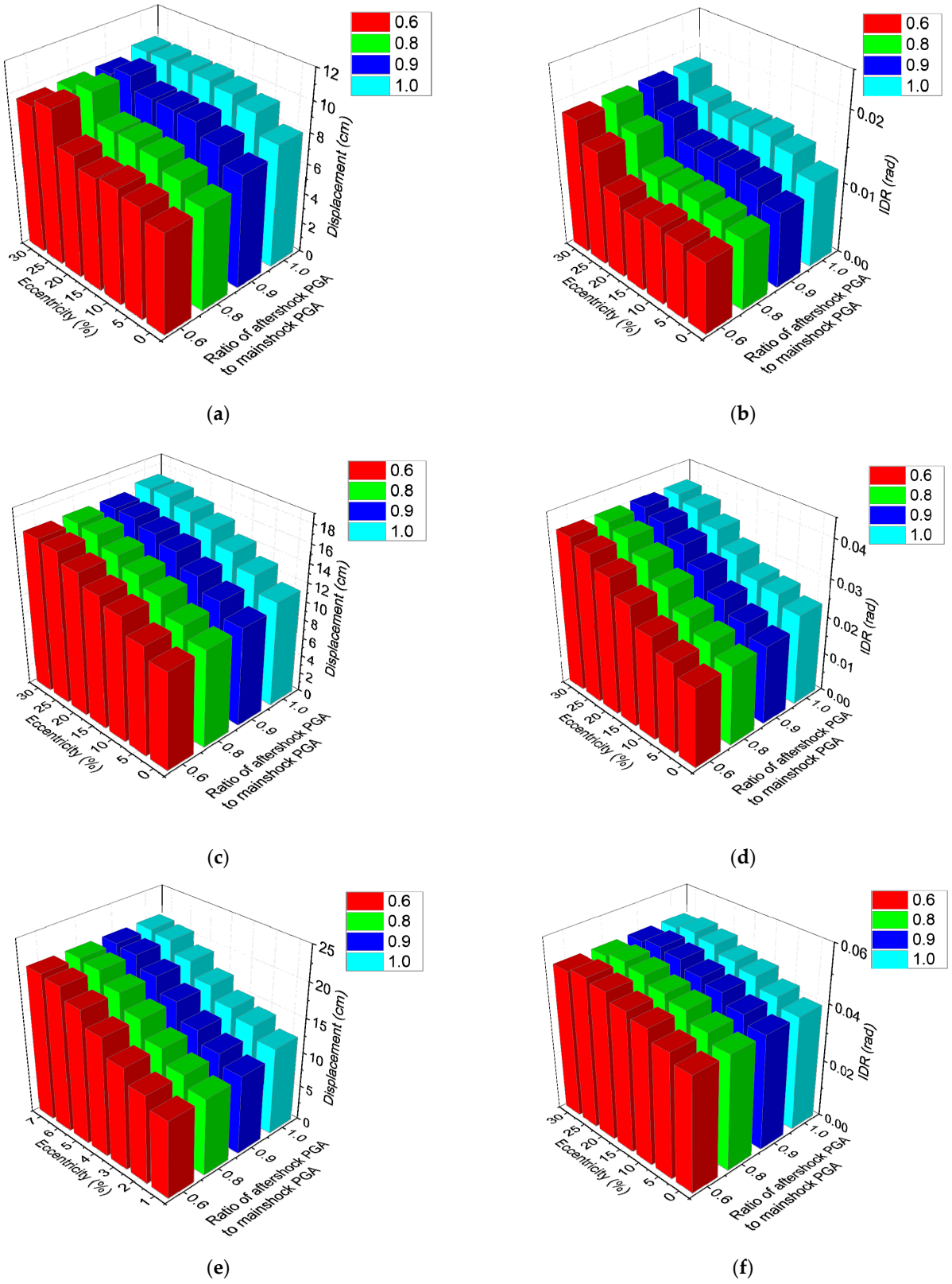



**Figure 13.** Seismic responses of structures under mainshock–aftershock sequences with different mainshock PGAs (case UUS): (**a**) Top floor maximum displacement with mainshock PGA at 0.15 g; (**b**) IDR with mainshock PGA at 0.15 g; (**c**) top floor maximum displacement with mainshock PGA at 0.25 g; (**d**) IDR with mainshock PGA at 0.25 g; (**e**) top floor maximum displacement with mainshock PGA at 0.32 g; (**f**) IDR with mainshock PGA at 0.32 g.

Moreover, the maximum displacements during the MSAS sequence and the mainshock are extracted. The ratios of structural maximum displacement during the MSAS sequence to that during the mainshock are presented in Figure 14a,c,e, corresponding to the mainshock PGAs which are 0.15 g, 0.25 g, and 0.32 g, respectively. Similarly, Figure 14b,d,f show the ratios of structural IDR during MSAS sequences to that during the mainshock when the mainshock PGAs are 0.15 g, 0.25 g, and 0.32 g, respectively.

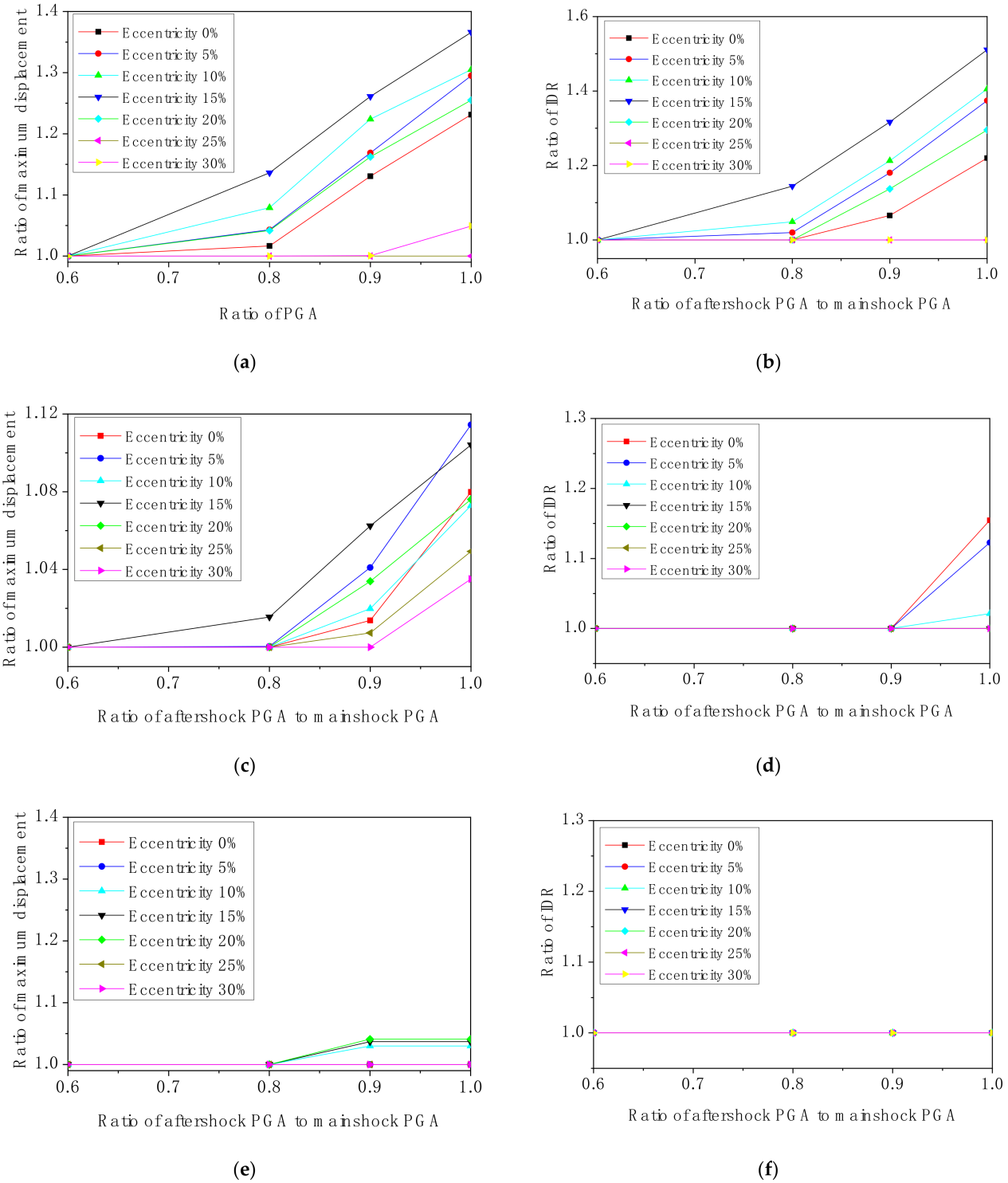



**Figure 14.** Ratios of maximum displacement and IDR under mainshock–aftershock sequences with different mainshock PGAs (case UUS): (**a**) Ratio of maximum displacement of aftershock to that of

mainshock with mainshock PGA at 0.15 g; (**b**) ratio of IDR of aftershock to that of mainshock with mainshock PGA at 0.15 g; (**c**) ratio of maximum displacement of aftershock to that of mainshock with mainshock PGA at 0.25 g; (**d**) ratio of IDR of aftershock to that of mainshock with mainshock PGA at 0.25 g; (**e**) ratio of maximum displacement of aftershock to that of mainshock with mainshock PGA at 0.32 g; (**f**) ratio of IDR of aftershock to that of mainshock with mainshock PGA at 0.32 g.

As illustrated in Figure 14a, at the same eccentricity, the ratio of aftershock displacement to mainshock displacement exceeds 1.0 and increases gradually with an increase in aftershock magnitude. It shows that the displacement during the aftershock is larger than that during the mainshock. When the scaling factor of aftershock amplitude is equal to 0.8, the displacement ratios increase significantly, except for the structural models with eccentricities of 25% and 30%. While the scaling factor is 1, the displacement ratios of almost all structures are increased, and the maximum ratio is increased by about 1.4 times. This means that if an aftershock with the same intensity as the mainshock (PGA 0.15 g) is encountered, there is a high probability that the displacement of the eccentric structure during the aftershock will exceed the maximum displacement during the mainshock. In addition, the amplification effect is more prominent in high eccentric structures, up to about 1.4 times more prominent.

Figure 14b indicates that the effect of aftershock on the 15% eccentricity structural model is the most significant. When the magnitude of aftershock is equal to that of the mainshock, the maximum IDR of the aftershocks is 1.5 times that of the mainshock. Compared with the displacement, the effect of scaled aftershocks can be more clearly reflected in the maximum IDR.

When the mainshock PGA is 0.25 g, as shown in Figure 14c, the ratios of the maximum displacement response show an upward trend with the increase in aftershock amplitude in each eccentricity. All the models' displacement response ratios significantly increase when the aftershock to mainshock ratio is 0.9, with the exception of the structural model with a 30% eccentricity. All structural models have significantly improved displacement response ratios when the mainshock to aftershock PGA ratio is 1. Among them, the displacement of the aftershock is, at most, 12% larger than that of the mainshock. This reflects that after experiencing a mainshock of 0.25 g, structures may suffer aggravated damage when loaded with aftershocks again of the same intensity. However, compared with structures experiencing a mainshock of small magnitude (i.e., 0.15 g), in the case of a mainshock of large magnitude, the influence of aftershocks on the structural model is significantly reduced.

Figure 14d presents that with an increase in eccentricity, the IDR grows obviously, and the growth rate slows down slightly at high eccentricity; structures with an eccentricity from 0% to 15% are more sensitive to the effects of aftershock than structures with higher eccentricity. When the scaling factor is less than 0.9, the maximum IDR of all structures during a scaled aftershock do not exceed that during the mainshock. However, when the scaling factor of aftershock amplitude is 1, the maximum IDR response in an aftershock is equal to 1.15 times that in the mainshock. Compared with the case of the structural model experiencing mainshock PGA = 0.15 g, the IDR responses in an aftershock can reach 1.5 times of that in the mainshock, when the mainshock PGA is 0.25 g. The results illustrate that the influence of aftershocks on the structural model is not as great as that of the former case, and it has little influence on the growth factor of IDR in aftershocks.

When the mainshock PGA is 0.32 g, the structural model's displacement rises as the eccentricity increases, but it does not change significantly as the aftershock amplitude changes when the eccentricity is the same. In Figure 14e, the aftershock displacement increases by less than 5%. The reason is as follows: When the structure is about to collapse, the prior damage caused by the mainshock to the structural model is so large that the effect of aftershock is negligible, which causes the displacement following the aftershock to possibly be less than the displacement after the mainshock.

For the maximum IDR, it similarly shows that the aftershock has little effect. As shown in Figure 14f, the response of structural models of eccentricity 0–25% also has an upward

trend, with the increase in eccentricity under the mainshock PGA being 0.32 g. However, the scaled aftershocks do not aggravate the structural damage directed by the index of maximum IDR. After loading the aftershock with the same intensity as the mainshock (0.32 g), the maximum IDR of the structure may not increase. The reason is that the structure already has experienced a large response under the mainshock, and even become severely damaged. Although the effect of scaled aftershocks does exist, it is still difficult to surpass the effect of the mainshock.

To sum up, with an increase in the mainshock PGA, the influence of aftershocks on the top floor maximum displacement and the maximum IDR of structures tend to decrease gradually. Compared with other mainshock PGAs, the effect of aftershock is most evident when the mainshock PGA is 0.15 g. The aftershock displacement of the structure reaches 1.4 times the mainshock displacement and the IDR reaches 1.5 times the mainshock displacement. When the mainshock PGA is 0.32 g, the response of the structure under the aftershock does not exceed the maximum response of the mainshock since the structure under the mainshock is close to destruction or even collapse.

#### 3.2.3. Response of Unidirectional Eccentric Structure under Bidirectional Mainshock

In this section, the seismic responses of the unidirectional eccentric structure under bidirectional mainshock–aftershock sequences (case UBM) are discussed. The influences of earthquake sequences and the eccentricity of structures on the structural seismic responses are discussed in this section. The difference is more significant in bidirectional earthquakes than in unidirectional earthquakes due to the coupled action of the translational mode and torsional mode, particularly in eccentric structures.

The earthquake ground motions are loaded along two horizontal directions, i.e., the X and Y directions. According to the seismic design code of buildings [34], the ratio of PGA of ground motion loaded in the X direction to that in the Y direction is set as 1:0.85. "CHICHI-CHY029-N" and "CHICHI-CHY029-E" are used to name the ground motions in the X direction and the Y direction, respectively. The PGAs in the X direction and Y direction are 0.238 g and 0.185 g, respectively.

In contrast to the displacement under bidirectional loading, as shown in Figure 15a, the Y direction displacement under unidirectional loading exhibits a similar upward trend with an increase in eccentricity. Additionally, when eccentricity is high, the growth rate slows. It is observed that the displacement of structural models with various eccentricities under bidirectional loading is larger than that under unidirectional loading, which shows that horizontal ground motion in the other direction (X direction) has an additional influence on the displacement in the Y direction. In Figure 15b, the residual displacements of structural models under unidirectional and bidirectional loadings are presented. It can be observed that the residual displacement increases in the overall trend with an improvement in eccentricity. But the residual displacement under biaxial loading is larger than that under unidirectional loading in small eccentricities, which demonstrates that the bidirectional horizontal ground motion has complex and adverse effects on the structural model. Figure 15c shows a comparison of the relative torsional effects on the structural model under unidirectional and bidirectional loadings. The relative torsional effects on the structural model almost increase linearly with an increase in eccentricity. Compared with the unidirectional loading, this parameter value of bidirectional loading is greater over the whole eccentricity range. Figure 15d illustrates the changing trend of torsional angles for structural models under unidirectional and bidirectional loadings. Although the torsional angle expresses the torsional behavior of a structure, it is still not a preferable index at several eccentricities. Both torsional angles seem to be the same. According to Figure 15a,c, with an increase in eccentricity, the torsional effect shows a trend of rising. In addition, the bidirectional loading causes more serious damage than unidirectional loading at each eccentricity. However, the torsional angle decreases at 30% eccentricity. Even at 5% eccentricity, the torsional angle of the bidirectional loading is smaller than that of the unidirectional loading.

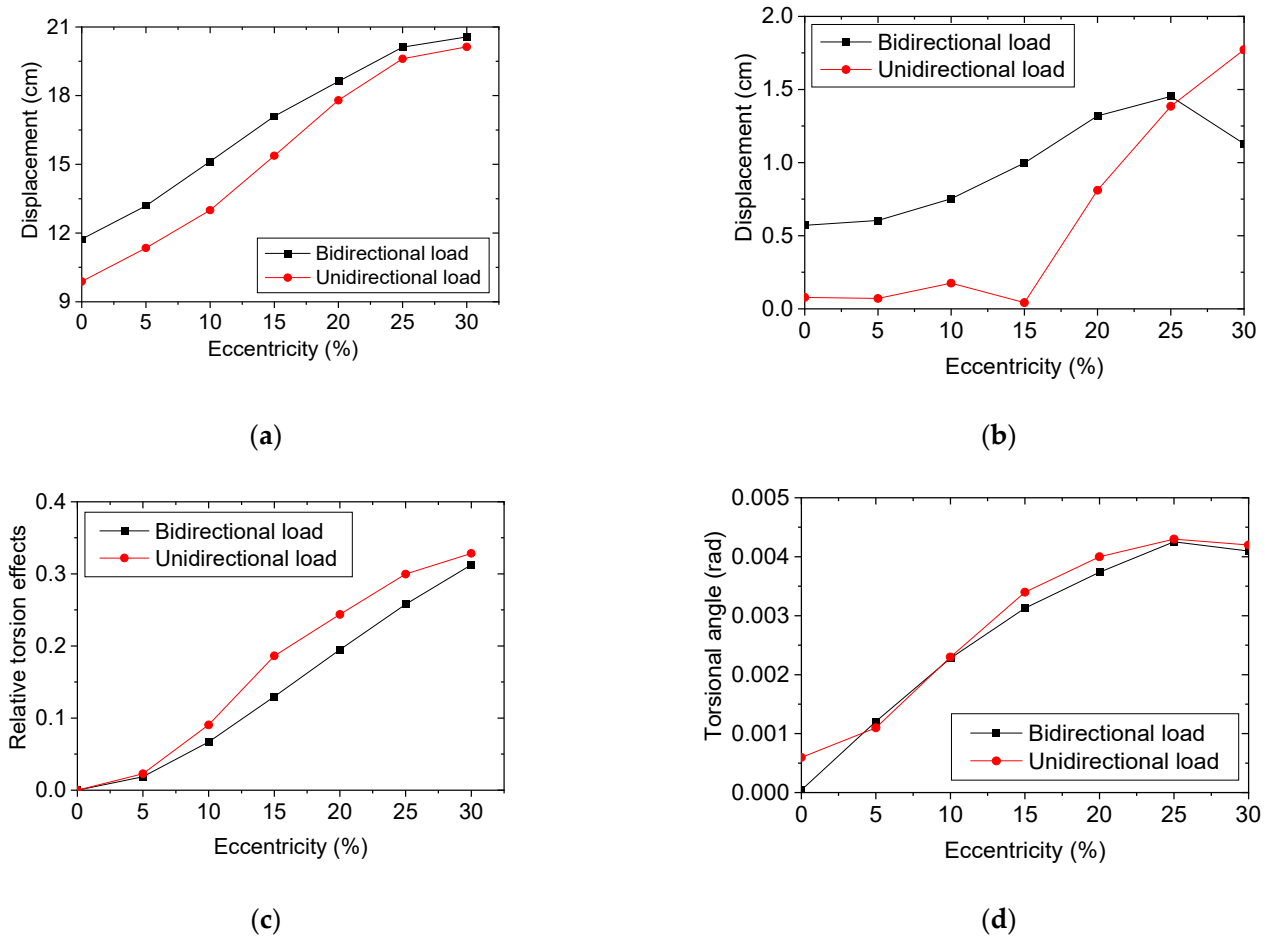



**Figure 15.** Response results of unidirectional eccentric structural models under bidirectional mainshock (case UBM): (**a**) Maximum displacements of top floor in Y direction; (**b**) residual displacements of top floor in Y direction; (**c**) relative torsional effects; (**d**) torsional angles.

#### 3.2.4. Response of the Unidirectional Eccentric Structure under Bidirectional Mainshock–Aftershock Sequences

The seismic responses of the unidirectional eccentric structure under bidirectional MSAS sequences (Case UBS) are explored. For the amplitude of the mainshock and aftershock, the mainshock PGAs are still 0.15 g, 0.25 g, and 0.32 g as determined above (Section 2.3), while the aftershock PGAs are still 0.6, 0.8, 0.9, and 1.0 times that of the mainshock. The amplitude of the ground motion loaded in the X direction is also 0.85 times that in the Y direction.

When the mainshock PGA is 0.15 g, as shown in Figures 16a and 17a, the structural displacement will increase with an increase in eccentricity under the same aftershock intensity. Compared with structures with different eccentricities, the symmetrical structure is most affected by the aftershock, and the maximum displacement under the aftershock is nearly 1.35 times of the mainshock displacement. If the structure eccentricity is larger, the effect of aftershock modulation amplitude is smaller. The IDRs of structures with eccentricities 0–30% under the bidirectional mainshock–aftershock sequences are shown in Figures 16b and 17b. Similarly, the IDR of the structure gradually increases with an increase in eccentricity, and the growth speed is rapid at high eccentricity. It is observed that the aftershock shows the most significant effect on the 0% eccentricity structure. When the aftershock amplitude is equal to the mainshock amplitude, the IDR of the aftershock is 1.3 times that of the mainshock.

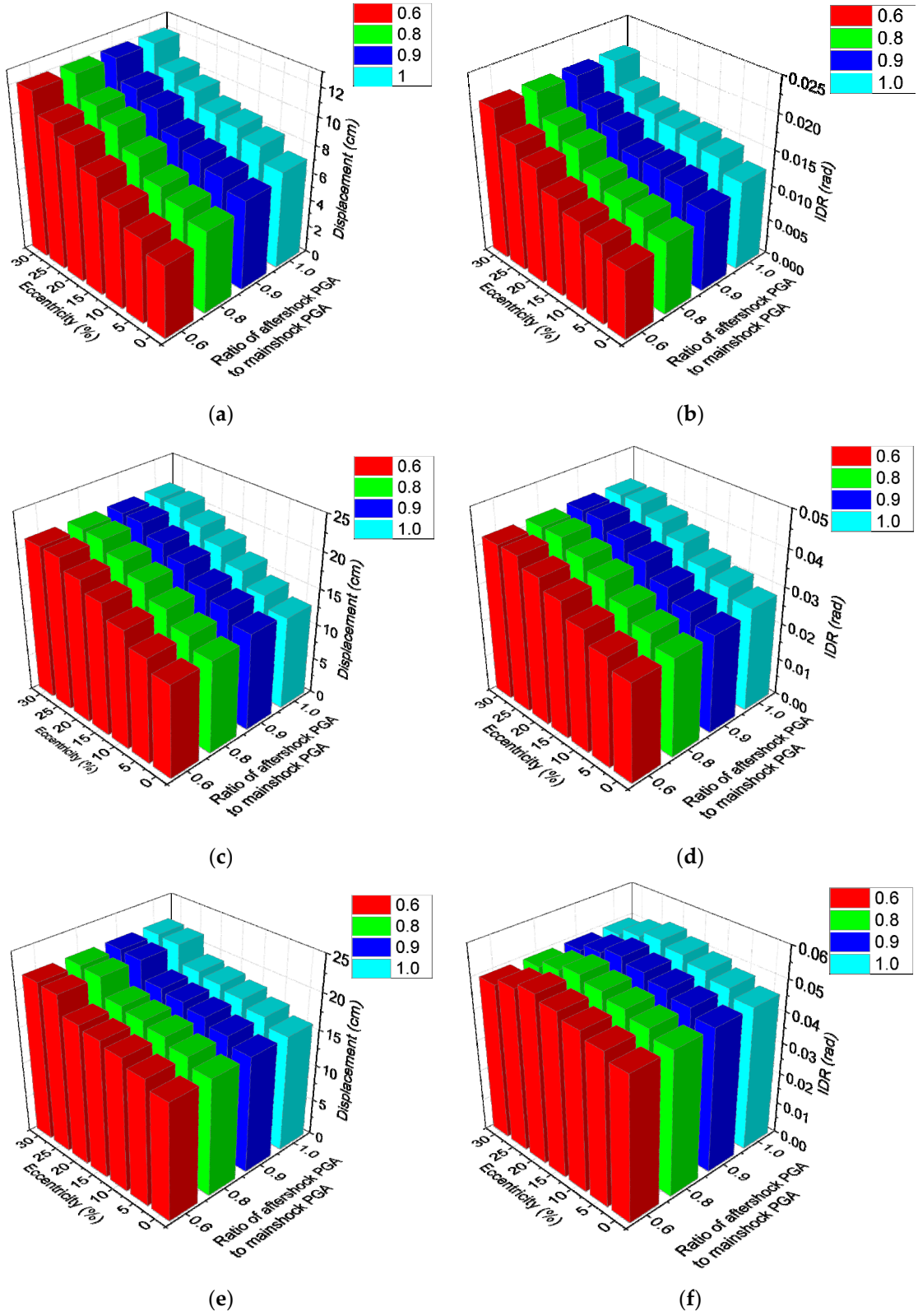
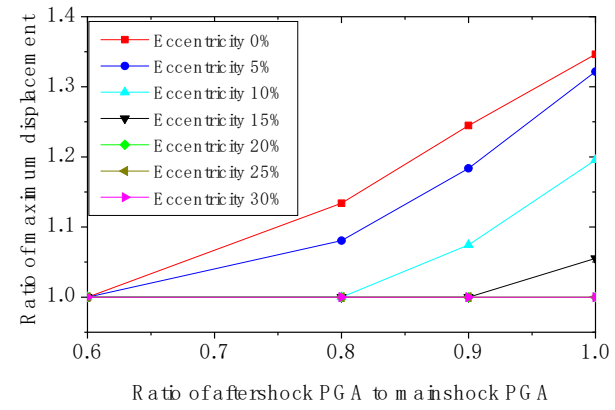
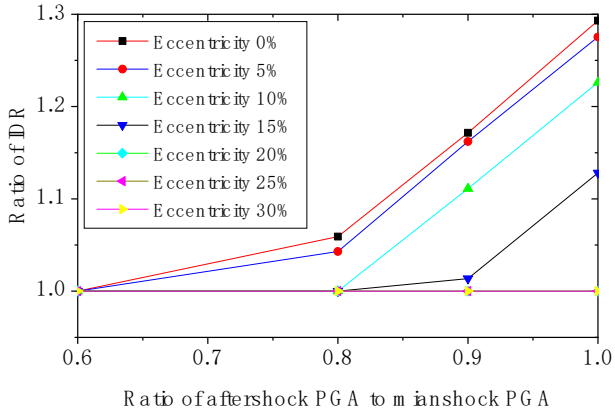


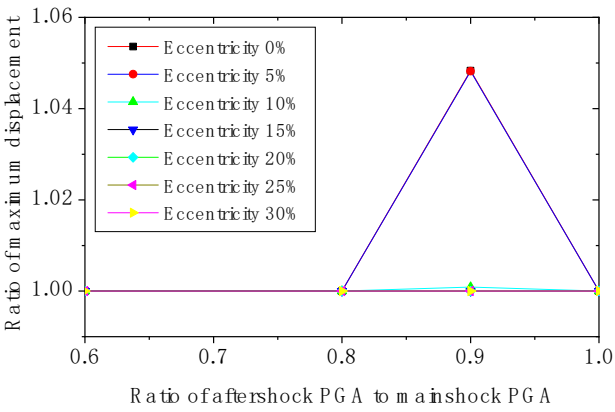

**Figure 16.** Seismic responses of structures under mainshock–aftershock sequences with different mainshock PGAs (case UBS): (**a**) Top floor maximum displacement with mainshock PGA at 0.15 g; (**b**) IDR with mainshock PGA at 0.15 g; (**c**) top floor maximum displacement with mainshock PGA at 0.25 g; (**d**) IDR with mainshock PGA at 0.25 g; (**e**) top floor maximum displacement with mainshock PGA at 0.32 g; (**f**) IDR with mainshock PGA at 0.32 g.



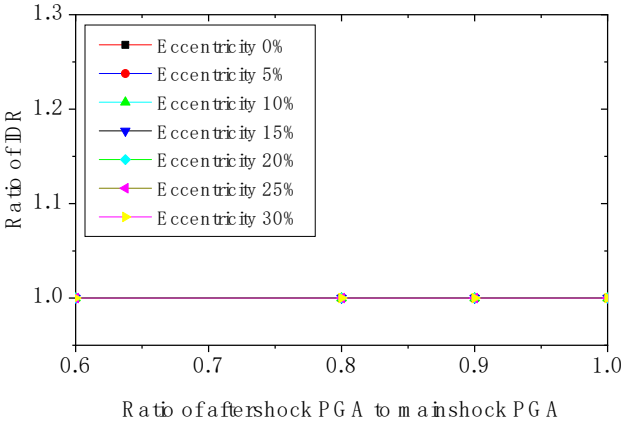

(**a**)



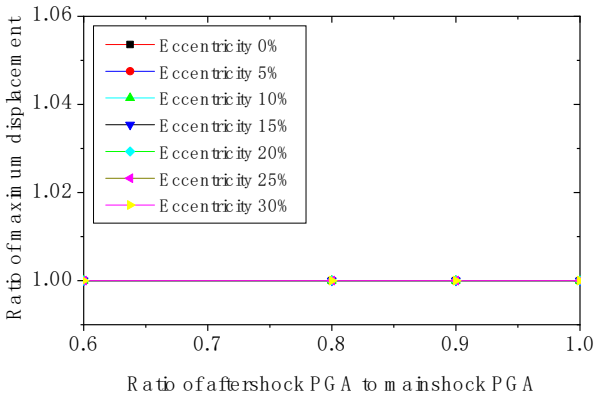

(**b**)



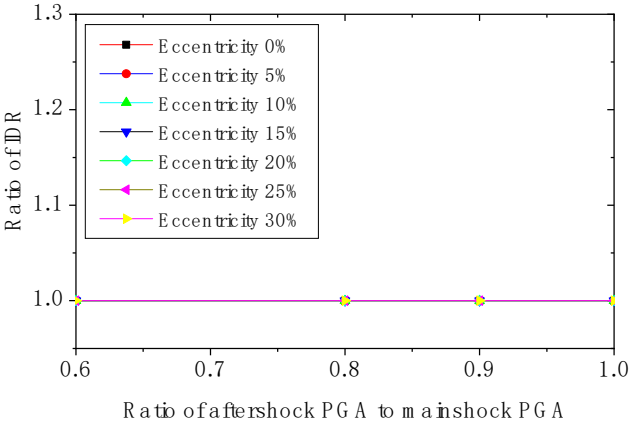

(**c**)




(**d**)




(**e**)




(**f**)

**Figure 17.** Ratios of maximum displacement and IDR of structures under mainshock–aftershock sequences with different mainshock PGAs (case UBS): (**a**) Ratio of maximum displacement of aftershock to that of mainshock with mainshock PGA at 0.15 g; (**b**) ratio of IDR of aftershock to that of mainshock with mainshock PGA at 0.15 g; (**c**) ratio of maximum displacement of aftershock to that of mainshock with mainshock PGA at 0.25 g; (**d**) ratio of IDR of aftershock to that of mainshock with mainshock PGA at 0.25 g; (**e**) ratio of maximum displacement of aftershock to that of mainshock with mainshock PGA at 0.32 g; (**f**) ratio of IDR of aftershock to that of mainshock with mainshock PGA at 0.32 g.

In the case of the mainshock, the PGA is 0.25 g, and the displacement growth speed slows down in the case of high eccentricity, as shown in Figure 16c. As illustrated in Figure 17c, despite the fact that the displacement of the structure with an eccentricity of 5% during the aftershock increased by 5% compared with that during the mainshock, the displacement of the other structures did not increase. It can be concluded that the aftershock shows a slight effect on eccentric structures with a life safety performance level. For the structural IDR, it can be seen in Figures 16d and 17d that the IDR of the aftershock cannot exceed that of the mainshock due to possible greater damage in mainshock loading.

For the mainshock PGA of 0.32 g, the aftershock fails to show an increasing effect on the structural displacement or IDR for structures with all the different eccentricities. It can be seen from Figure 17e,f that the aftershock displacements of all structures did not exceed the mainshock displacements. This shows that the structure tends to be damaged after the first earthquake of a larger amplitude, and at this time, the aftershock response does not manage to exceed the mainshock.

The reason could be that the structure's response to the bidirectional mainshock is already extremely large and its performance level at 0.32 g under the mainshock reaches collapse prevention. In the structure with high eccentricity (i.e., 30%), the IDR decreased, which showed that the structure had been damaged seriously or even collapsed. Therefore, the response of the aftershock can hardly exceed that of the mainshock.

In summary, it can be concluded that, similar to the unidirectional loading, with an increase in the mainshock PGA, the influence of aftershock on the structural maximum displacement and IDR will decrease. When the mainshock PGA is 0.15 g, the aftershock shows the most significant influence on the structural response. During the aftershock, the maximum displacement of the top floor is more than 1.35 times of the mainshock, and the IDR is 1.3 times.

### *3.3. Seismic Dynamic Analyses of Bidirectional Eccentric Structures*

#### 3.3.1. Response of Bidirectional Eccentric Structure under Bidirectional Mainshock

In this section, the seismic analyses of bidirectional eccentric structures under bidirectional mainshock (case BBM) are studied. The earthquake ground motions used in the case are the same as the aforementioned earthquake records, i.e., the "CHICHI-CHY029-N" and "CHICHI-CHY029-E" earthquake records. The eccentric structural models used in the case are bidirectional eccentric models which are developed by a unidirectional eccentric structure. Both of them have the same eccentricity. The mass center of the bidirectional eccentric structure is adjusted along the x-axial and y-axial directions at the same time.

The seismic responses of unidirectional and bidirectional eccentric structures with different eccentricities are compared. As shown in Figure 18, the overall trend of the bidirectional eccentric structure increases with the improvement in eccentricity. The increasing trend is more obvious in the Y direction than that in the X direction. Comparing unidirectional eccentric structure and bidirectional eccentric structure, after loading the same bidirectional earthquakes, the displacement trend of unidirectional eccentric structure is positively correlated with the eccentricity, probably a linear relationship, while the bidirectional eccentric structure is more complex.

Moreover, the torsional angles of the unidirectional eccentric structure and the bidirectional eccentric structure are presented in Figure 19. It can be seen that both torsional angles climb upward with an increase in eccentricity. This indicates that the torsional effect of the bidirectional eccentric structure is slightly larger than that of the unidirectional eccentric structure.

#### 3.3.2. Response of the Bidirectional Eccentric Structure under Bidirectional Mainshock–Aftershock Sequences

The seismic responses of the bidirectional eccentric structure under bidirectional mainshock–aftershock sequences (case BBS) are further examined through a dynamic analysis. The maximum displacement responses of the structures are presented in Figure 20a,c,e.

To investigate the influence of aftershock, the ratios of the maximum displacement under the MSAS sequences to the displacement under the mainshock are also compared, which are shown in Figure 21a,c,e. It can be demonstrated that structures with small eccentricities are more sensitive to aftershocks, and the maximum impact of aftershocks on displacement can reach 1.5 times that of the mainshock (at the mainshock PGA 0.15 g). But, for high PGAs of the mainshock (i.e., 0.25 g and 0.32 g), aftershocks have little impact on the structural displacement. Only for symmetrical structures and structures with small eccentricities, such as 5% eccentric structures, could aftershocks increase the displacement response, but the increase effect is less than 5%.

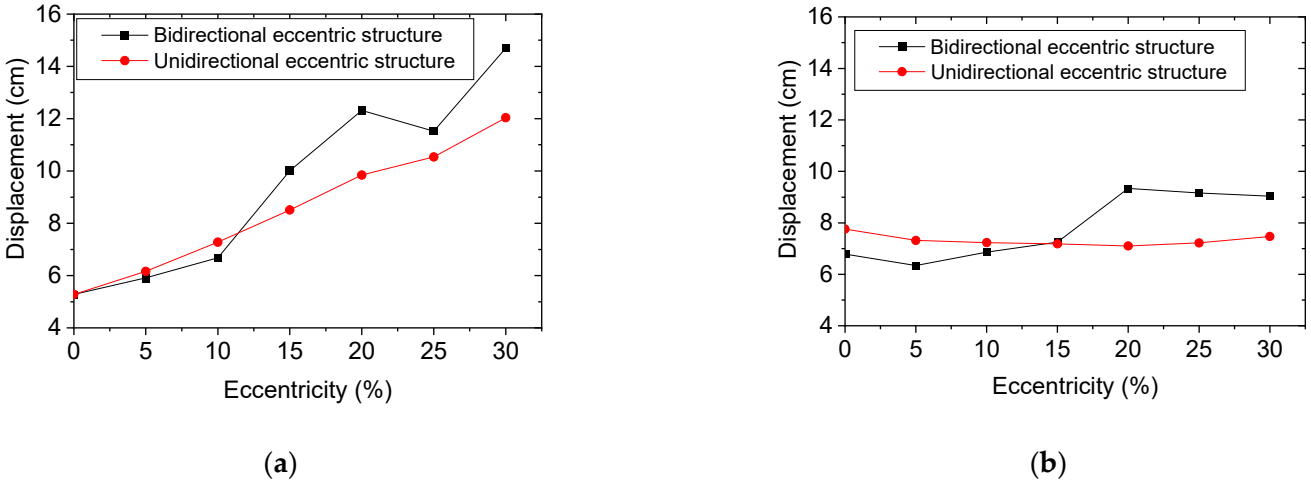



**Figure 18.** Comparison of top floor displacement of unidirectional eccentric structure and bidirectional eccentric structure with different eccentricities: (**a**) Top floor displacement in the Y direction; (**b**) top floor displacement in the X direction.

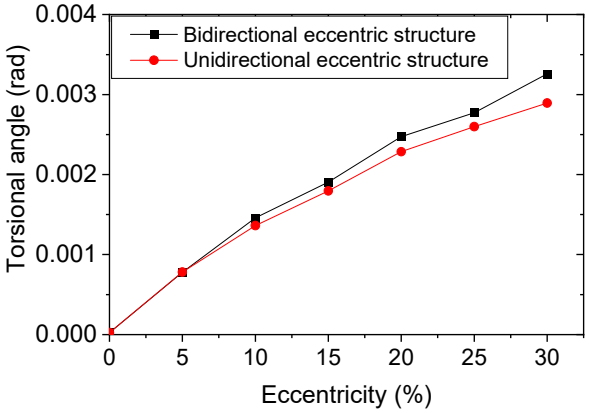



**Figure 19.** Comparison of the torsional angles between the unidirectional eccentric structure and the bidirectional eccentric structure.

As illustrated in Figure 20b,d,f, with an improvement in eccentricity, the IDR increases obviously and uniformly at eccentricities of 0~15%, increases slowly at eccentricities of 1~25%, and decreases at the stage of 25~30%. The influence of aftershocks on IDR is only reflected in the structures with an eccentricity of 0% and 5%, which is similar to the maximum displacement response. Figure 21b,d,f also show that when the mainshock PGA is 0.15 g, the aftershock IDR can reach up to 1.4 times that of the mainshock. However, the aftershock IDR is about 1.06 times the mainshock IDR in the case of a mainshock PGA of 0.25 g, and equal to zero time in the case of a mainshock PGA of 0.32 g.

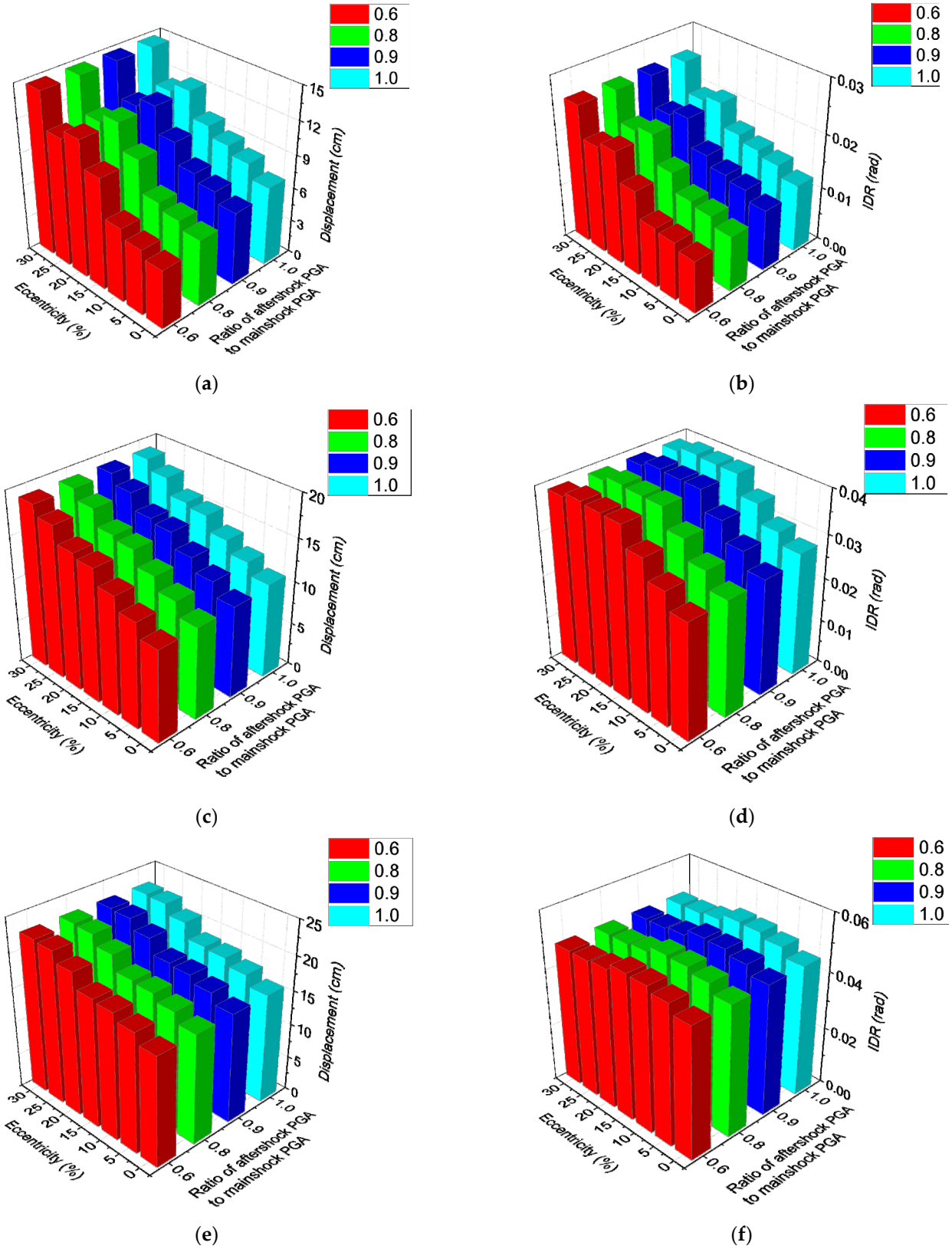



**Figure 20.** Seismic responses of structures under mainshock–aftershock sequences with different mainshock PGAs (case BBM): (**a**) Top floor maximum displacement with mainshock PGA at 0.15 g; (**b**) IDR with mainshock PGA at 0.15 g; (**c**) top floor maximum displacement with mainshock PGA at 0.25 g; (**d**) IDR with mainshock PGA at 0.25 g; (**e**) top floor maximum displacement with mainshock PGA at 0.32 g; (**f**) IDR with mainshock PGA at 0.32 g.

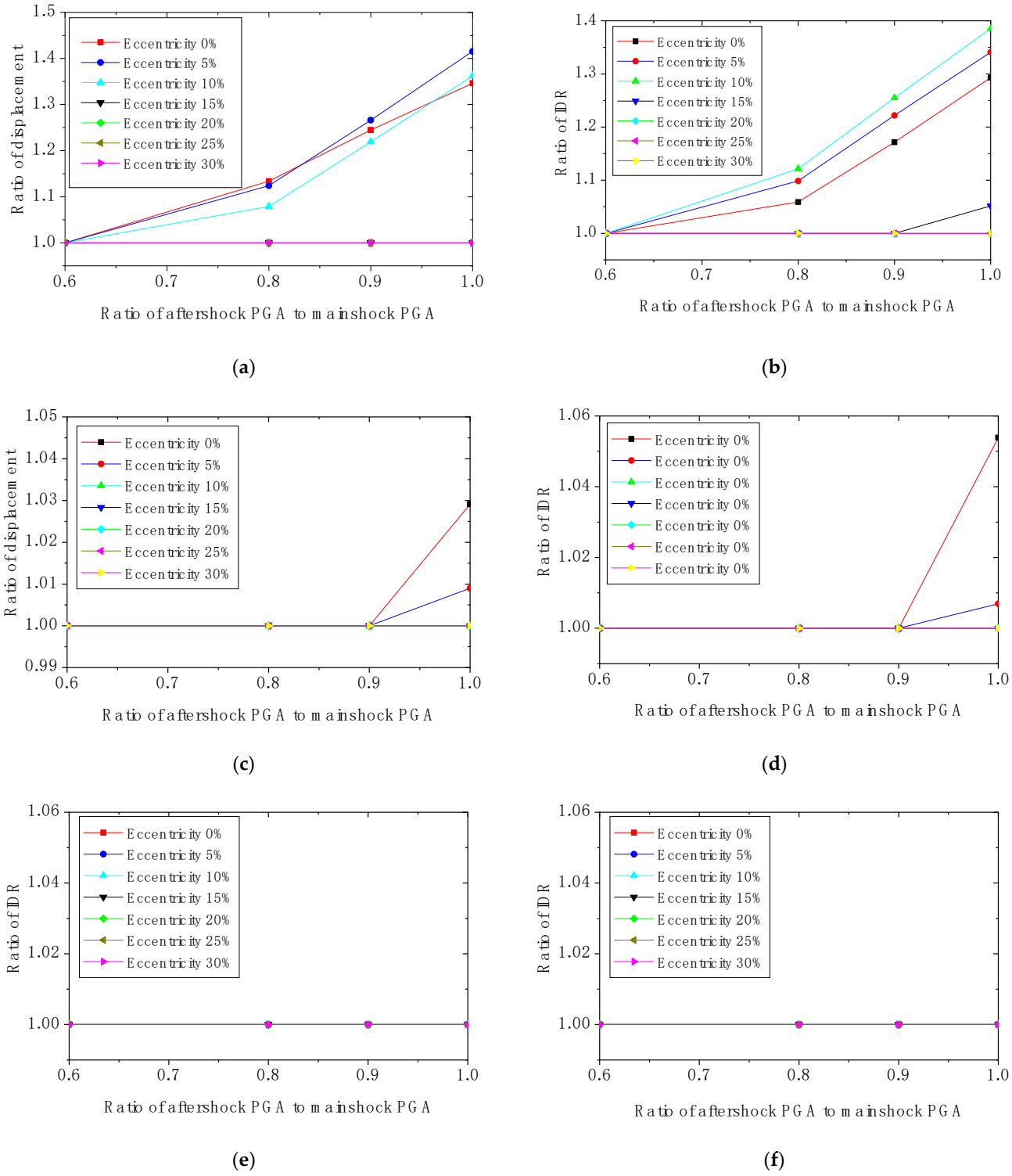



**Figure 21.** Ratios of maximum displacement and IDR of structures under mainshock–aftershock sequences with different mainshock PGAs (case BBS): (**a**) Ratio of maximum displacement of aftershock to that of mainshock with mainshock PGA at 0.15 g; (**b**) ratio of IDR of aftershock to that of mainshock with mainshock PGA at 0.15 g; (**c**) ratio of maximum displacement of aftershock to that of mainshock with mainshock PGA at 0.25 g; (**d**) ratio of IDR of aftershock to that of mainshock with mainshock PGA at 0.25 g; (**e**) ratio of maximum displacement of aftershock to that of mainshock with mainshock PGA at 0.32 g; (**f**) ratio of IDR of aftershock to that of mainshock with mainshock PGA at 0.32 g.

In addition, compared with the unidirectional eccentric structure, the influence of aftershock on the bidirectional structure is obviously greater. It is noted that in Figures 16f and 20f, when the mainshock PGA is 0.32 g, the IDR response decreased at high eccentricities of 15–30%, which was different from the general increasing situations. The reason is that the bidirectional structure has a greater response than the unidirectional eccentric structure in the bidirectional 0.32 g mainshock. The IDR of the structure with an eccentricity of 30% decreases, indicating that the structure is damaged or even collapsed. In this case, it is difficult for the aftershock to exceed the effect of the mainshock, even if the aftershock amplitude is equal to the mainshock amplitude.

Consequently, for the bidirectional eccentric structures, with an increase in the mainshock PGA, the influence of aftershocks on the maximum displacement and the IDR of the structures are decreased. When the mainshock PGA is 0.15 g, the effect of aftershock is the most significant. The maximum displacement of the structure is about 1.5 times greater than that of the mainshock, and the IDR is around 1.4 times greater than that of the mainshock. However, when the mainshock PGAs are 0.25 g and 0.32 g, the impact of aftershocks on the structure is weakened or even not present. The reason is that the bidirectional eccentric structures are close to destruction or even collapse under such strong mainshocks. Meanwhile, compared with the unidirectional eccentric structures, it is demonstrated that aftershocks have a greater impact on the bidirectional eccentric structures under the same bidirectional loading.

## 4. Conclusions

This study investigates the effects of aftershocks on seismic responses of unidirectional eccentric structures and bidirectional eccentric structures with different eccentricities subjected to unidirectional and bidirectional loadings. In the investigation, three-dimensional models of unidirectional and bidirectional eccentric structures with eccentricities of 0%, 5%, 10%, 15%, 20%, 25%, and 30% are established by using the OpenSEES software. A representative mainshock–aftershock sequence is selected and scaled according to the performance level indicated by the IDR. Seismic capacities of the symmetric structural models and eccentric structural models are estimated by a static pushover analysis and a nonlinear time history analysis. Seismic response results under a total of six types of cases (called UUM, UUS UBM, UBS, BBM, and BBS) are discussed. The main conclusions are as follows:

1. For unidirectional eccentric structures, the displacement response during the unidirectional mainshock increases obviously with an improvement in eccentricity, and the displacement growth rate increases first and then decreases. The structural response increases further under the unidirectional MSAS. The peak displacement and maximum inter-story drift ratio during the aftershock can reach up to 1.4 times and 1.5 times those of the mainshock, respectively, when the structure experiences a mainshock of 0.15 g. When the amplitude of the mainshock is low, the aftershock shows a more significant influence on the structural response.
2. For unidirectional eccentric structures, bidirectional horizontal loadings are more likely to cause damage to the structures and have a more adverse effect on the structural displacement responses in the main direction. The symmetric structure is most affected by the aftershock under the bidirectional MSAS. The peak displacement and maximum inter-story drift ratio during the aftershock can reach up to 1.35 times and 1.3 times those of the mainshock, respectively, when the structure experiences a mainshock of 0.15 g. Compared with the structural response under bidirectional loading, the structural response under unidirectional loading is more sensitive to the intensity of aftershock ground motions.
3. For bidirectional eccentric structures, the peak displacements and maximum inter-story drift ratios of the structures tend to ascend with an increase in eccentricity. Compared with unidirectional eccentric structures, the responses of bidirectional eccentric structures are more complex under the same bidirectional horizontal earth-

quakes, and the aftershocks have a more significant influence on the responses of bidirectional eccentric structures. When the structure experienced a mainshock of 0.15 g, the peak displacement during the aftershock can reach 1.5 times that of the mainshock, and the maximum inter-story drift ratio during the aftershock can reach 1.4 times that of the mainshock.

The non-synchronous nonlinear behaviors of different columns of the perimeter frames may have an influence on the change in eccentricities, which need to have further investigations. Different nonlinear behaviors of columns could produce different increased trends of structural demands (i.e., torsional angle and inter-story drift ratio).

**Author Contributions:** Investigation, P.S.; methodology, P.S. and W.W.; project administration, W.W.; supervision, W.W.; writing—original draft preparation, P.S. and S.Z.; writing—review and editing, P.S., S.Z. and W.W. All authors have read and agreed to the published version of the manuscript.

**Funding:** This investigation is supported by the National Natural Science Foundation of China (Nos. 52222811, U1939210, and 52178469), Natural Science Foundation of Heilongjiang Province (No. LH2021E075), the Fundamental Research Funds for the Central Universities (No. HIT.BRET.2022010). These supports are greatly appreciated.

**Data Availability Statement:** No new data were created or analyzed in this study. Data sharing is not applicable to this article.

**Conflicts of Interest:** The authors declare no conflict of interest. The opinions and conclusions presented in this paper are those of the authors and do not necessarily reflect the views of the sponsoring organizations.

## References

1. Li, X.; Zhou, Z.; Yu, H.; Wen, R.; Lu, D.; Huang, M.; Zhou, Y.; Cu, J. Strong motion observations and recordings from the great Wenchuan Earthquake. *Earthq. Eng. Eng. Vib.* **2008**, *7*, 235–246. [CrossRef]
2. Zhai, C.-H.; Wen, W.-P.; Li, S.; Chen, Z.; Chang, Z.; Xie, L.-L. The damage investigation of inelastic SDOF structure under the mainshock–aftershock sequence-type ground motions. *Soil Dyn. Earthq. Eng.* **2014**, *59*, 30–41. [CrossRef]
3. Fragiacomo, M.; Amadio, C.; Macorini, L. Seismic response of steel frames under repeated earthquake ground motions. *Eng. Struct.* **2004**, *26*, 2021–2035. [CrossRef]
4. Hatzigeorgiou, G.D.; Liolios, A.A. Nonlinear behaviour of RC frames under repeated strong ground motions. *Soil Dyn. Earthq. Eng.* **2010**, *30*, 1010–1025. [CrossRef]
5. Brown, R.D.; Ward, P.L. Geologic and seismologic aspects of the managua, nicaragua, earthquakes of December 23, 1972. *Bull. Seismol. Soc. Am.* **1974**, *64*, 1031. [CrossRef]
6. Goel, R.K.; Chopra, A.K. Inelastic seismic response of one-storey, asymmetric-plan systems: Effects of stiffness and strength distribution. *Earthq. Eng. Struct. Dyn.* **1990**, *19*, 949–970. [CrossRef]
7. Jiang, W.; Hutchinson, G.L.; Wilson, J.L. Inelastic torsional coupling of building models. *Eng. Struct.* **1996**, *18*, 288–300. [CrossRef]
8. Reyes, J.C.; Kalkan, E. Should ground-motion records be rotated to fault-normal/parallel or maximum direction for response history analysis of buildings. *US Geol. Surv. Open-File Rep.* **2012**, *1261*, 89.
9. Kalkan, E.; Reyes, J.C. Significance of rotating ground motions on behavior of symmetric-and asymmetric-plan structures: Part II. Multi-story structures. *Earthq. Spectra* **2015**, *31*, 1613–1628. [CrossRef]
10. Kosmopoulos, A.J.; Fardis, M.N. Estimation of inelastic seismic deformations in asymmetric multistorey RC buildings. *Earthq. Eng. Struct. Dyn.* **2010**, *36*, 1209–1234. [CrossRef]
11. Buratti, N.; Minghini, F.; Ongaretto, E.; Savoia, M.; Tullini, N. Empirical seismic fragility for the precast RC industrial buildings damaged by the 2012 Emilia (Italy) earthquakes. *Earthq. Eng. Struct. Dyn.* **2017**, *46*, 2317–2335. [CrossRef]
12. Ruggieri, S.; Chatzidaki, A.; Vamvatsikos, D.; Uva, G. Reduced-order models for the seismic assessment of plan-irregular low-rise frame buildings. *Earthq. Eng. Struct. Dyn.* **2022**, *51*, 3327–3346. [CrossRef]
13. Ruggieri, S.; Uva, G. Accounting for the Spatial Variability of Seismic Motion in the Pushover Analysis of Regular and Irregular RC Buildings in the New Italian Building Code. *Buildings* **2020**, *10*, 177. [CrossRef]
14. Bhasker, R.A. A seismic fragility model accounting for torsional irregularity in low-rise non-ductile RC moment resisting frame buildings. *Earthq. Eng. Struct. Dyn.* **2021**, *51*, 912–934. [CrossRef]
15. Manie, S.; Moghadam, A.S.; Ghafory-Ashtiany, M. Collapse response assessment of low-rise buildings with irregularities in plan. *Earthq. Struct.* **2015**, *9*, 49–71. [CrossRef]
16. Michalis, F.; Dimitrios, V.; Manolis, P. Evaluation of the influence of vertical irregularities on the seismic performance of a nine-storey steel frame. *Cornell Univ. Press* **2006**, *35*, 1489–1509. [CrossRef]

17. Sayyed, O.; Kushwah, S.S.; Rawat, A. Seismic Analysis of Vertical Irregular RC Building with Stiffness and Setback Irregularities. *IOSR J. Mech. Civ. Eng.* **2017**, *14*, 40–45. [CrossRef]
18. Lee, H.S.; Ko, D.W. Seismic Response Characteristics of High-Rise RC Wall Buildings Having Different Irregularities in Lower Stories. *Steel Constr.* **2007**, *29*, 3149–3167. [CrossRef]
19. Bilgin, H.; Urui, R. Effects of structural irregularities on low and mid-rise RC building response. *J. Struct. Mech.* **2018**, *4*, 33. [CrossRef]
20. Pant, D.R.; Wijeyewickrema, A.C. Performance of base-isolated reinforced concrete buildings under bidirectional seismic excitation considering pounding with retaining walls including friction effects. *Earthq. Eng. Struct. Dyn.* **2014**, *43*, 1521–1541. [CrossRef]
21. Kohrangi, M.; Bazzurro, P.; Vamvatsikos, D. Conditional spectrum bidirectional record selection for risk assessment of 3D structures using scalar and vector IMs. *Earthq. Eng. Struct. Dyn.* **2019**, *48*, 1066–1082. [CrossRef]
22. Yamamoto, M.; Minewaki, S.; Yoneda, H.; Higashino, M. Nonlinear behavior of high-damping rubber bearings under horizontal bidirectional loading: Full-scale tests and analytical modeling. *Earthq. Eng. Struct. Dyn.* **2012**, *41*, 1845–1860. [CrossRef]
23. Yang, Z.D.; Lam, E.S. Dynamic responses of two buildings connected by viscoelastic dampers under bidirectional earthquake excitations. *Earthq. Eng. Eng. Vib.* **2014**, *13*, 137–150. [CrossRef]
24. Grant, D.N. Response Spectral Matching of Two Horizontal Ground-Motion Components. *J. Struct. Eng.* **2011**, *137*, 289–297. [CrossRef]
25. Lee, H.S.; Hwang, K.R. Torsion design implications from shake-table responses of an RC low-rise building model having irregularities at the ground story. *Earthq. Eng. Struct. Dyn.* **2014**, *44*, 907–927. [CrossRef]
26. De Domenico, D.; Losanno, D.; Vaiana, N. Experimental tests and numerical modeling of full-scale unbonded fiber reinforced elastomeric isolators (UFREIs) under bidirectional excitation. *Eng. Struct.* **2023**, *274*, 115118. [CrossRef]
27. Hosseinpour, F.; Abdelnaby, A.E. Effect of different aspects of multiple earthquakes on the nonlinear behavior of RC structures. *Soil Dyn. Earthq. Eng.* **2017**, *92*, 706–725. [CrossRef]
28. Oyguc, R.; Toros, C.; Abdelnaby, A.E. Seismic behavior of irregular reinforced-concrete structures under multiple earthquake excitations. *Soil Dyn. Earthq. Eng.* **2018**, *104*, 15–32. [CrossRef]
29. *GB 18306-2015*; Construction, C.M.o. Seismic Ground Motion Parameter Zonation Map of China. China Earthquake Administration: Beijing, China, 2015.
30. McKenna, F. OpenSees: A framework for earthquake engineering simulation. *Comput. Sci. Eng.* **2011**, *13*, 58–66. [CrossRef]
31. Kent Dudley, C.; Park, R. Flexural Members with Confined Concrete. *J. Struct. Div.* **1971**, *97*, 1969–1990. [CrossRef]
32. Menegotto, M. Method of analysis for cyclically loaded RC plane frames including changes in geometry and non-elastic behavior of elements under combined normal force and bending. In *Proceedings of the IABSE Symposium on Resistance and Ultimate Deformability of Structures Acted on by Well Defined Repeated Loads*; Istituto di Scienza e Tecnica delle Costruzioni Univerita di: Roma, Italy, 1973; pp. 15–22.
33. Spacone, E.; Filippou, F.C.; Taucer, F.F. Fibre beam–column model for non-linear analysis of R/C frames: Part I. *Formulation. Earthq. Eng. Struct. Dyn.* **1996**, *25*, 711–725. [CrossRef]
34. *GB50011-2010*; Construction, C.M.o. Code for Seismic Design of Buildings. Ministry of Housing and Urban-Rural Construction of the People's Republic of China: Beijing, China, 2010.


**Disclaimer/Publisher's Note:** The statements, opinions and data contained in all publications are solely those of the individual author(s) and contributor(s) and not of MDPI and/or the editor(s). MDPI and/or the editor(s) disclaim responsibility for any injury to people or property resulting from any ideas, methods, instructions or products referred to in the content.